Mechanisms of Concurrent Hydride Migration Processes in a Triruthenium Cluster Capped by a Phenylphosphinidene (PPh) Ligand

Antony J. Deeming*[a] Caroline S. Forth,[a] Md. Iqbal Hyder,[b] Shariff E. Kabir,*[b] Ebbe Nordlander*[c] Fiona Rodgers[a] and Bettina Ullmann[c]

Keywords: Ruthenium / Clusters / Hydrides / Dynamic mobility / Kinetics

Two methods were used to synthesise $[Ru_3(\mu\text{-}H)_2(\mu_3\text{-}PPh)(CO)_7(\mu\text{-}dppm)]$ (**3**) (dppm = $Ph_2PCH_2PPh_2$), the subject of this paper. Treatment of $[Ru_3(CO)_{10}(\mu\text{-}dppm)]$ (**1**) with phenylphosphane in refluxing THF gave both $[Ru_3(\mu\text{-}H)(\mu\text{-}PHPh)(CO)_8(\mu\text{-}dppm)]$ (**2**) and $[Ru_3(\mu\text{-}H)_2(\mu_3\text{-}PPh)(CO)_7(\mu\text{-}dppm)]$ (**3**). Cluster **2** converts to **3** in refluxing THF. Alternatively the phenylphosphinidene cluster $[Ru_3(\mu\text{-}H)_2(\mu_3\text{-}PPh)(CO)_9]$ (**4**), prepared by the reported method of treating $[Ru_3(CO)_{12}]$ with phenylphosphane, reacts with dppm to produce cluster **3**. The single-crystal X-ray structures of **2** and **3** are reported. Hydride mobility in $[Ru_3(\mu\text{-}H)_2(\mu_3\text{-}PPh)(CO)_7(\mu\text{-}dppm)]$ (**3**) was analysed by variable-temperature ^1H and $^{31}P\{^1H\}$ NMR methods. The variations in the spectra with temperature could not be interpreted by a single process, several of which were explored and which gave inadequately matching computed and experimental spectra. However, the spectra were successfully analysed by two concurrent processes, both involving the migration of hydride ligands between Ru–Ru edges. The faster process leads to the exchange of the nonequivalent phosphorus nuclei but not hydride exchange, whereas the hydrides are also exchanged in the slower process. Both processes require hydride ligand migration from one Ru–Ru edge to a vacant one. The hydride ligand bridging the same pair of ruthenium atoms as the dppm ligand is the slower to migrate.

(© Wiley-VCH Verlag GmbH & Co. KGaA, 69451 Weinheim, Germany, 2005)

Introduction

Hydride migration between edge-bridging, face-bridging and terminal sites in transition-metal clusters has been commonly observed.[1] It is possible to probe these migrations by NMR coalescence and other classical methods if the hydride ligands are inequivalent, by changes in the appearance of coupling patterns to the metal centres if there is a spin-active metal nucleus, or by exchanges in sites within another ligand that result from hydride migration. The phosphinidene-capped cluster $[Ru_3(\mu\text{-}H)_2(\mu_3\text{-}PPh)(CO)_9]$[2–4] (**4**) presumably has mobile hydride ligands which can undergo degenerate migrations from either of the two occupied edges to the vacant one. To the best of our knowledge this has never been demonstrated although in related clusters, such as $[Os_3(\mu\text{-}H)_2(\mu_3\text{-}S)(CO)_9]$, this type of process has been investigated.[5] By introducing phosphane ligands into $[Ru_3(\mu\text{-}H)_2(\mu_3\text{-}PPh)(CO)_9]$ (**4**), the hydrides may become inequivalent and distinguishable hydride migrations of different rate might occur. The hydride ligands will preferentially occupy some sites rather than others, in particular the bridging sites between the most electron-rich metal centres. Migration of hydrides out of electron-rich sites into electron-poor sites is likely to be slow.

In this paper we will describe in detail the fluxional behaviour of the cluster $[Ru_3(\mu\text{-}H)_2(\mu_3\text{-}PPh)(CO)_7(\mu\text{-}dppm)]$ (**3**) which has C_1 symmetry. There are inequivalent hydrides and three inequivalent ^{31}P nuclei so that NMR analysis of the fluxional behaviour is straightforward.

Results and Discussion

Synthesis and Characterisation of Compounds

We used two different methods to synthesise compound **3** from $[Ru_3(CO)_{12}]$ as shown in Scheme 1. The introduction of the diphosphane (dppm) ligand first followed by treatment of $[Ru_3(CO)_{10}(dppm)]$ (**1**)[6] with Ph_2PH in refluxing THF, gave both $[Ru_3(\mu\text{-}H)(\mu\text{-}PHPh)(CO)_8(\mu\text{-}dppm)]$ (**2**) and $[Ru_3(\mu\text{-}H)_2(\mu_3\text{-}PPh)(CO)_7(\mu\text{-}dppm)]$ (**3**), which were easily separated and characterised. There was no improvement in the reaction of **1** with $PhPH_2$ when Me_3NO was employed to remove CO ligands by oxidation. Thermal treatment of **2** in refluxing THF leads to **3**, and presumably this is the route by which **3** is formed as shown in Scheme 1.

Alternatively, the PPh ligand may be introduced in the first step to form $[Ru_3(\mu\text{-}H)_2(\mu_3\text{-}PPh)(CO)_9]$ **4** from Ph_2PH and $[Ru_3(CO)_{12}]$ by known methods.[2–4] Cluster **4** may then

[a] Department of Chemistry, University College London, 20 Gordon Street, London, UK WC1H 0AJ
E-mail: a.j.deeming@ucl.ac.uk
[b] Department of Chemistry, Jahangirnagar University, Savar, Dhaka 1342, Bangladesh
[c] Inorganic Chemistry, Center for Chemistry and Chemical Engineering, Lund University, Box 124, 22100 Lund, Sweden

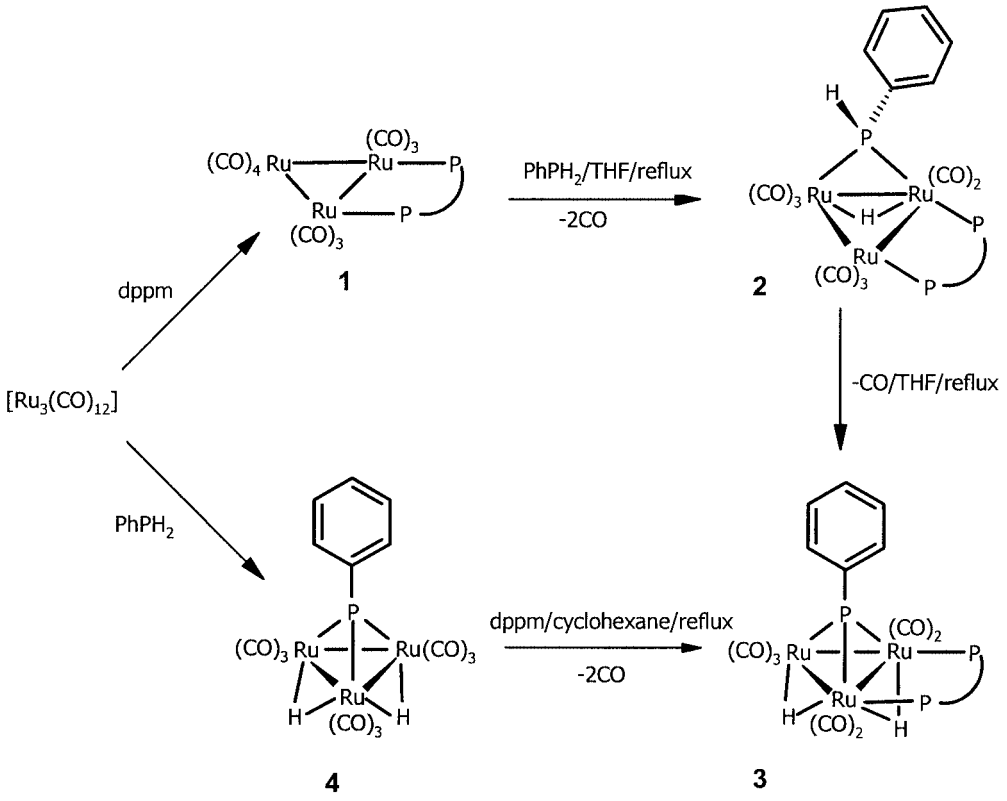

Scheme 1.

be substituted by dppm. This substitution was attempted unsuccessfully by preparing MeCN derivatives of the type $[Ru_3(\mu\text{-}H)_2(\mu_3\text{-}PPh)(CO)_{9-x}(MeCN)_x]$ (x = 1 or 2), followed by treatment of these in situ with dppm. Likewise a photochemical procedure (UV) for the reaction of $[Ru_3(\mu\text{-}H)_2(\mu_3\text{-}PPh)(CO)_9]$ (**4**) with dppm was attempted. Neither of these methods gave much product. However, direct thermal treatment of **4** with dppm leads to the two products: $[Ru_3(\mu\text{-}H)_2(\mu_3\text{-}PPh)(CO)_7(\mu\text{-}dppm)]$ (**3**) and a minor yellow band which gave $[Ru_3(\mu\text{-}H)_2(\mu_3\text{-}PPh)(CO)_8(\mu\text{-}dppm)]$. The latter complex readily looses CO to form **3**, and we have been unable to characterise it fully. We believe it contains a monodentate dppm ligand. This was indicateded by its IR spectrum around 2000 cm^{-1}, which is very closely similar to that of monodentate phosphane derivatives such as $[Ru_3(\mu\text{-}H)_2(\mu_3\text{-}PPh)(CO)_8(PMe_2Ph)]$.[7,8]

Characterisation of Compound 2

The single-crystal XRD structure of cluster **2** is shown in Figure 1. Crystal data are in Table 1 and some selected geometric data are in Table 2. The framework of the compound corresponds to that of $[Ru_3(\mu\text{-}H)(\mu\text{-}PHPh)(CO)_{10}]$ with the H and the PHPh ligands spanning the same Ru–Ru edge.[2] The hydride ligand was located from diffraction data. The dppm ligand, however, bridges one of the other two Ru–Ru edges, unlike the structure of $[Os_3(\mu\text{-}H)_2(CO)_8(\mu\text{-}dppm)]$ in which the three bridging ligands are at the same Os–Os edge.[9] The structure of **2** is essentially as expected for this arrangement of ligands but there are some bond lengths worth noting. Atom Ru(3) is the most heavily substituted by P-donors but is associated with the shorter Ru–P bonds. For the PHPh ligand, Ru(3)–P(1) [2.3069(12) Å] is shorter than Ru(1)–P(1) [2.3490(12) Å] and for dppm, Ru(3)–P(2) [2.2998(11) Å] is shorter than Ru(2)–P(3) [2.3245(12) Å]. If, as one would expect, Ru(3) is the most electron-rich centre, the bond lengths could be explained by greater π donation by that atom to the phosphorus ligands. One should also note that Ru–CO distances *trans* to the μ-PHPh ligand are long and Ru–CO distances *trans* to μ-H are short with respect to the other related distances in this molecule. The bridging dppm has negligible impact on the length of the Ru–Ru bond compared to the unbridged edge; 2.8494(10) Å compared with 2.8509(8) Å.

In the light of this structure, there are some problems in accounting for the ^1H NMR spectra. The IR and mass spectra are completely consistent with the solid-state structure but the NMR spectrum seems to indicate higher symmetry than that in the crystal. The hydride appears as a 1:2:1 triplet at δ = –16.30 ppm and the CH_2 hydrogen atoms appear as a single triplet at δ = 4.26 ppm. Neither of these observations are predicted from the XRD structure. The spectra at –50 °C as well as at 27 °C show these features so we believe the compound is non-fluxional. The CH_2 triplet must be due to accidental isochronicity and the observed triplet for the hydride signal is probably due to similar coupling to the two non-equivalent ^{31}P nuclei at Ru(3)

 © 2005 Wiley-VCH Verlag GmbH & Co. KGaA, Weinheim

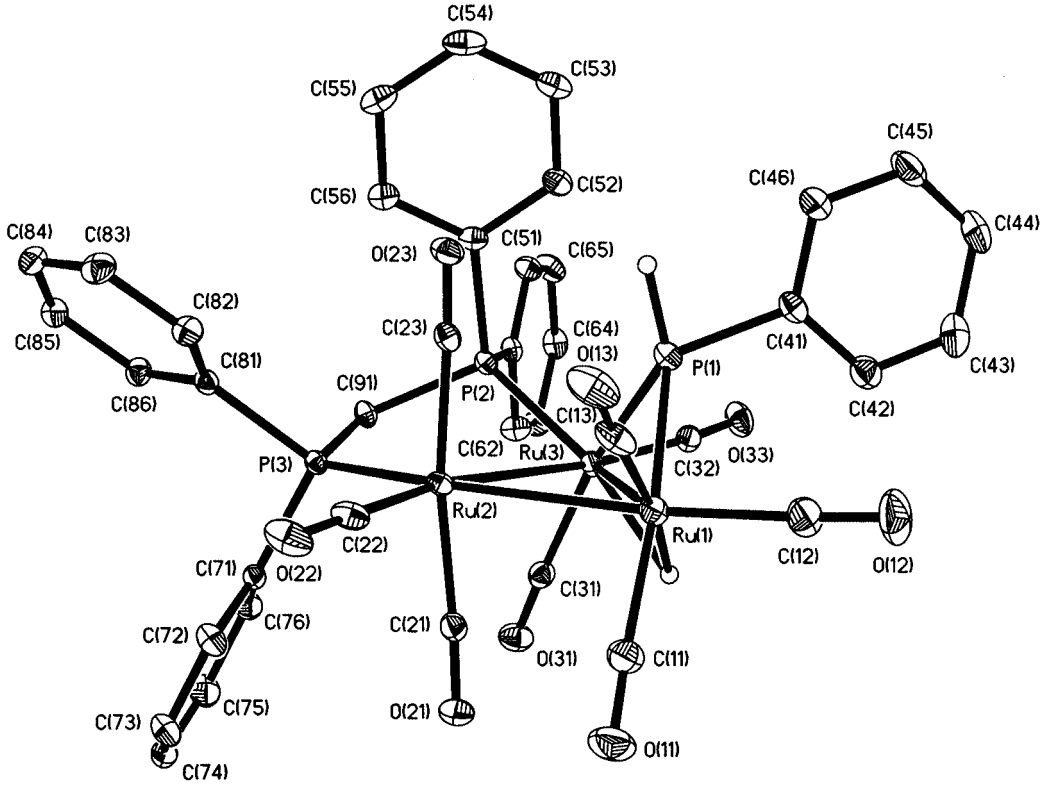

Figure 1. Molecular structure of $[Ru_3(\mu\text{-H})(\mu\text{-PHPh})(CO)_8(\mu\text{-dppm})]$ (**2**). H atoms on phenyl rings were omitted.

Table 1. Crystal data and structure refinement for the clusters $[Ru_3(\mu\text{-H})(\mu\text{-PHPh})(CO)_8(\mu\text{-dppm})]$ (**2**) and $[Ru_3(\mu\text{-H})_2(\mu_3\text{-PPh})(CO)_7(\mu\text{-dppm})]$ (**3**).

	2	**3**
Chemical formula	$C_{39}H_{29}O_8P_3Ru_3$	$C_{38}H_{29}O_7P_3Ru_3$
Formula mass	1021.74	993.73
Temperature [K]	150(2)	293(2)
Crystal system, space group	triclinic, $P\bar{1}$	monoclinic, $P2_1/n$
a [Å]	11.524(4)	17.4429(12)
b [Å]	12.337(4)	12.8386(9)
c [Å]	15.278(6)	17.7454(12)
α [°]	112.940(5)	90
β [°]	92.037(6)	92.1310(10)
γ [°]	106.155(6)	90
Cell volume [Å^3]	1895.6(12)	3971.2(5)
Z	2	4
Calcd. density [g cm^{-3}]	1.790	1.662
Abs. coeff. μ [mm^{-1}]	1.359	1.293
$F(000)$	1008	1960
Crystal colour	orange-red	yellow
Crystal size [mm]	0.46 × 0.13 × 0.11	0.43 × 0.33 × 0.23
θ range for data collection [°]	1.47 to 28.41	1.61 to 28.30
Index ranges	h –15/15, k –16/16, l –19 /19	h –22/22, k –17/17, l –23/23
Completeness to θ	91.5% to 28.41	99.9% to 26.00°
Reflections collected	16773	34723
Independent reflections	8740 (R_{int} = 0.0231)	9530 (R_{int} = 0.0211)
Reflections with $F^2 > 2\sigma$	7935	8382
Min. and max. transmission	0.5744 and 0.8705	0.6070 and 0.7571
Structure solution	Patterson synthesis	Direct methods
Weighting parameters a, b	0.0337, 4.9084	0.0401, 1.3354
Data/restraints/parameters	8740/0/484	9530/0/466
Final R indices [$F^2 > 2\sigma$]	R_1 = 0.0384, wR_2 = 0.0921	R_1 = 0.0315, wR_2 = 0.0752
R indices (all data)	R_1 = 0.0427, wR_2 = 0.0946	R_1 = 0.0376, wR_2 = 0.0784
Goodness-of-fit on F^2	1.073	1.061
Largest and mean shift/su	0.001 and 0.000	0.004 and 0.000
Largest diff. peak and hole [e·Å^{-3}]	2.716 and –1.515	0.486 and –0.332

 © 2005 Wiley-VCH Verlag GmbH & Co. KGaA, Weinheim

Table 2. Selected bond lengths [Å] and angles [°] for the compound $[Ru_3(\mu\text{-H})(\mu\text{-PHPh})(CO)_8(\mu\text{-dppm})]$ (**2**).

Ru(1)–Ru(2)	2.8509(8)	Ru(1)–P(1)–Ru(3)	77.62(4)
Ru(1)–Ru(3)	2.9183(10)	Ru(2)–Ru(3)–P(2)	86.22(3)
Ru(2)–Ru(3)	2.8494(10)	Ru(3)–Ru(2)–P(3)	92.38(3)
Ru(1)–P(1)	2.3490(12)	P(1)–Ru(3)–P(2)	101.91(4)
Ru(3)–P(1)	2.3069(12)	P(1)–Ru(1)–C(13)	92.68(13)
Ru(3)–P(2)	2.2998(11)	Ru(1)–Ru(2)–P(3)	153.74(3)
Ru(2)–P(3)	2.3245(12)	Ru(1)–Ru(3)–P(2)	136.40(3)

which are not resolved, together perhaps with virtual coupling effects.

Characterisation of $[Ru_3(\mu\text{-H})_2(\mu_3\text{-PPh})(CO)_7(\mu\text{-dppm})]$ (3)

The single-crystal XRD structure of cluster **3** is shown in Figure 2 and some selected geometric data are listed in Table 3. The structure is based on that known for $[Ru_3(\mu\text{-H})_2(\mu_3\text{-PPh})(CO)_9]$.[2] The dppm ligand bridges in equatorial sites at Ru(1) and Ru(2) with all three P nuclei on the same side of the Ru_3 plane. The hydride ligands are located on the Ru(1)–Ru(2) and Ru(1)–Ru(3) edges consistent with these bonds being longer than Ru(2)–Ru(3). ^{1}H NMR spectroscopic data at 233 K and $^{31}P\{^1H\}$ NMR spectroscopic data at 213 K show all three ^{31}P nuclei are in different environments and that the hydrides are non-equivalent. The P nuclei of the dppm ligand both lie equatorially (*cis* to the PPh ligand) and it is the hydride locations that make the dppm unsymmetrical.

Analysis of VT ^{1}H and $^{31}P\{^1H\}$ NMR spectra for $[Ru_3(\mu\text{-H})_2(\mu_3\text{-PPh})(CO)_7(\mu\text{-dppm})]$ (3)

Figure 3 shows that the $^{31}P\{^1H\}$ NMR spectrum for $[Ru_3(\mu\text{-H})_2(\mu_3\text{-PPh})(CO)_7(\mu\text{-dppm})]$ (**3**) at 213 K contains a double doublet at δ = 277.75 for the phosphinidene ligand and two doublets of doublets at δ = 25.20 and 27.70 ppm for the inequivalent dppm phosphorus nuclei. Changes oc-

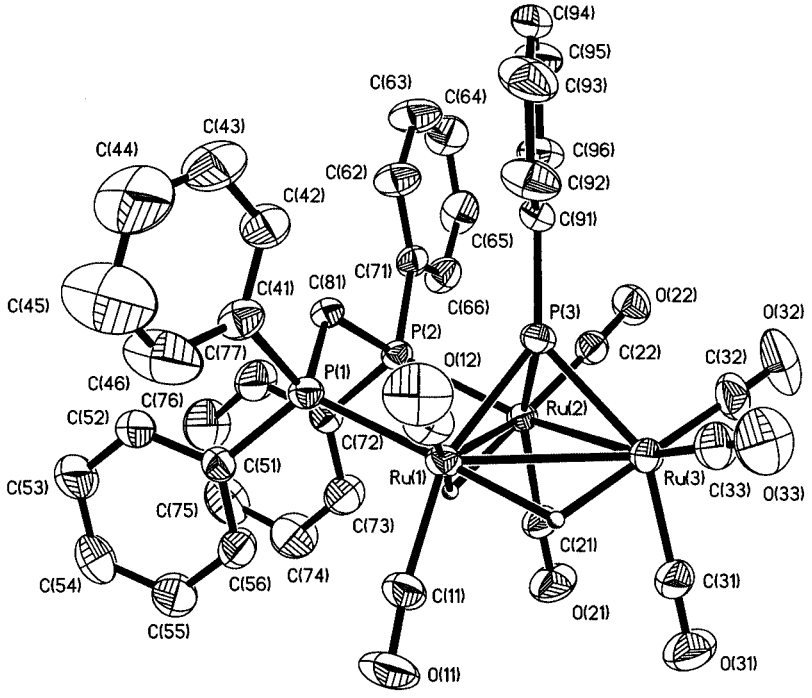

Figure 2. Molecular structure of $[Ru_3(\mu\text{-H})_2(\mu_3\text{-PPh})(CO)_7(\mu\text{-dppm})]$ (**3**). H atoms on phenyl rings were omitted.

Table 3. Selected bond lengths [Å] and angles [°] for the compound $[Ru_3(\mu\text{-H})_2(\mu_3\text{-PPh})(CO)_7(\mu\text{-dppm})]$ (**3**).

Ru(1)–Ru(2)	2.9351(3)	Ru(1)–P(3)–Ru(2)	79.40(2)
Ru(1)–Ru(3)	2.9428(4)	Ru(1)–P(3)–Ru(3)	79.21(2)
Ru(2)–Ru(3)	2.8317(3)	Ru(2)–P(3)–Ru(3)	76.55(2)
Ru(1)–P(3)	2.3196(7)	Ru(1)–Ru(2)–P(2)	93.724(18)
Ru(2)–P(3)	2.2750(7)	Ru(2)–Ru(1)–P(1)	90.406(18)
Ru(3)–P(3)	2.2964(7)	P(1)–Ru(1)–P(3)	96.36(2)
Ru(1)–P(1)	2.3205(7)	P(2)–Ru(2)–P(3)	99.35(2)
Ru(2)–P(2)	2.3140(7)		

 © 2005 Wiley-VCH Verlag GmbH & Co. KGaA, Weinheim

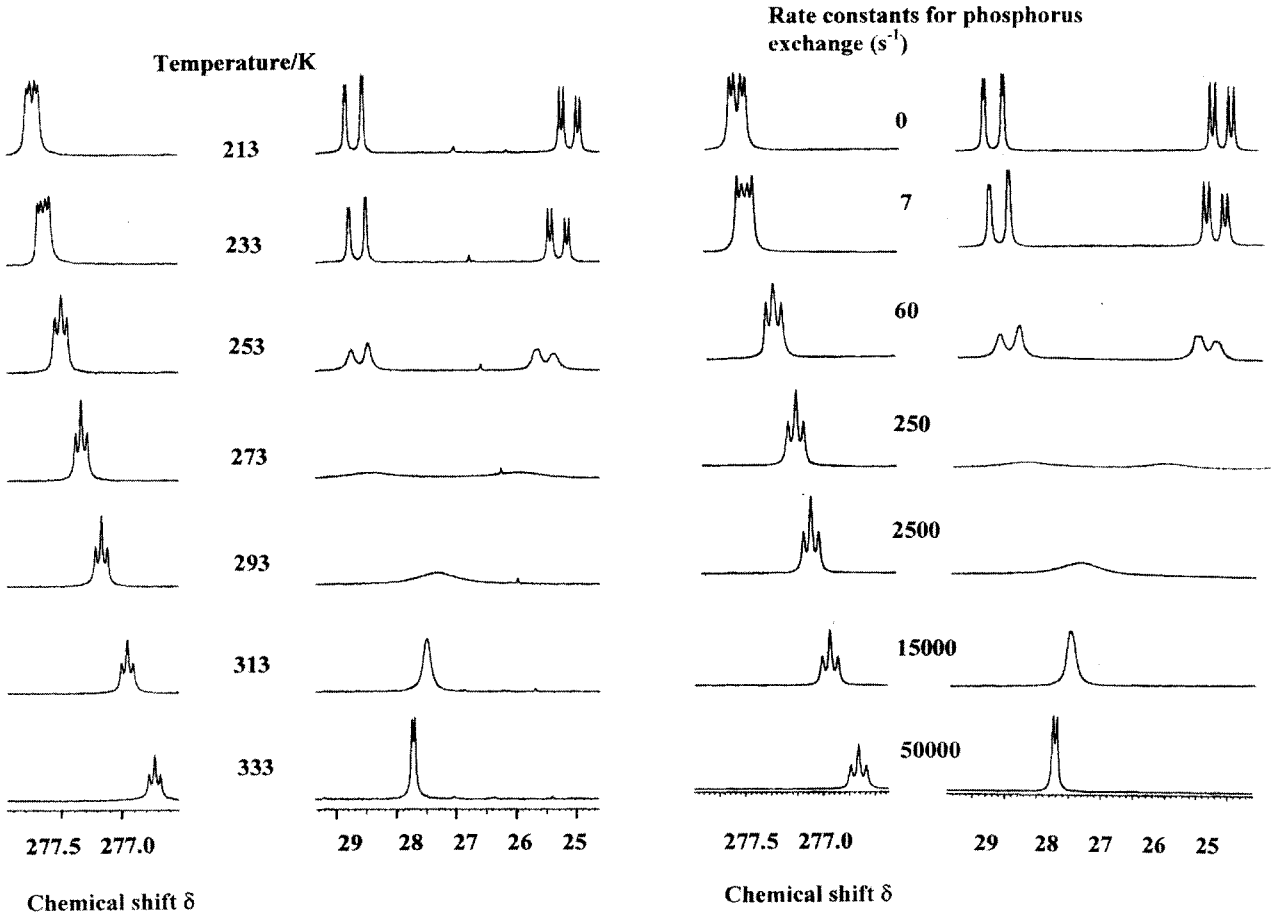

Figure 3. Spectra on left: observed 202.5 MHz $^{31}P\{^1H\}$ NMR spectra of $[Ru_3(\mu\text{-}H)_2(\mu_3\text{-}PPh)(CO)_7(\mu\text{-}dppm)]$ (**3**) in $CDCl_3$ recorded at the various temperatures given. Spectra on right: corresponding $^{31}P\{^1H\}$ NMR spectra of **3** simulated using gNMR at the given rate constants for phosphorus–phosphorus exchange.

cur as the temperature is raised. The dppm signals broaden and coalesce at about 260 K forming a doublet at 333 K. The phosphinidene converts from a double doublet to a 1:2:1 triplet over the same temperature range. These observations are consistent with the exchange of the phosphorus atoms of the dppm resulting from hydride mobility. This was confirmed by a accurate simulation of the $^{31}P\{^1H\}$ NMR spectra (using gNMR[10]) also shown in Figure 3 which gives the rates used to simulate the spectra. It was also necessary to change the chemical shifts somewhat with temperature to produce an accurate simulation. The simplest intramolecular process to account for the observations is shown in Scheme 2.

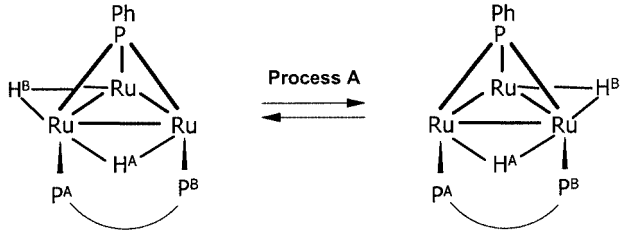

Scheme 2.

Process A does not lead to hydride exchange. This wastested by recording the hydride spectrum over a temperature range (Figure 4). The ^1H NMR spectrum for the hydrides of $[Ru_3(\mu\text{-}H)_2(\mu_3\text{-}PPh)(CO)_7(\mu\text{-}dppm)]$ at 333 K is a single doublet (with an indication of a small triplet pattern at each branch of the doublet). The crystal structure indicates that the hydrides should be non-equivalent, and at 233 K the hydride spectrum appears as a complex multiplet (at least 10 peaks resolved) (see Figure 4). We were able to model this multiplet satisfactorilly by two overlapping multiplets for the non-equivalent hydride ligands at δ = –18.450 and –18.466 ppm, and the NMR shifts and coupling constants used in these simulations are given in Table 4. By using the data in Table 4 we obtained good agreement between observed and calculated spectra at the low-temperature limit (233 K for ^1H and 213 K for ^{31}P). The overlap of hydride signals made it difficult to follow coalescence. We attempted to simulate the spectra on the basis of various exchange processes. Figure 4 shows spectra predicted by process A in Scheme 2. Clearly the hydrides are not exchanging so two overlapping multiplets are found even at the highest rates. Hydride exchange is required to give the observed high-temperature spectra. Figure 4 show the spec-

 © 2005 Wiley-VCH Verlag GmbH & Co. KGaA, Weinheim

tra expected on the basis of the exchange of hydride nuclei alone without any other exchange occurring. A single resonance is obtained but very different from that observed. We also simulated spectra on the basis of process B shown in Scheme 3. The central configuration with a plane of symmetry is not detectably populated at any time and is not observed in the low-temperature spectra. Hence we cannot descriminate process B from one in which there is synchro-

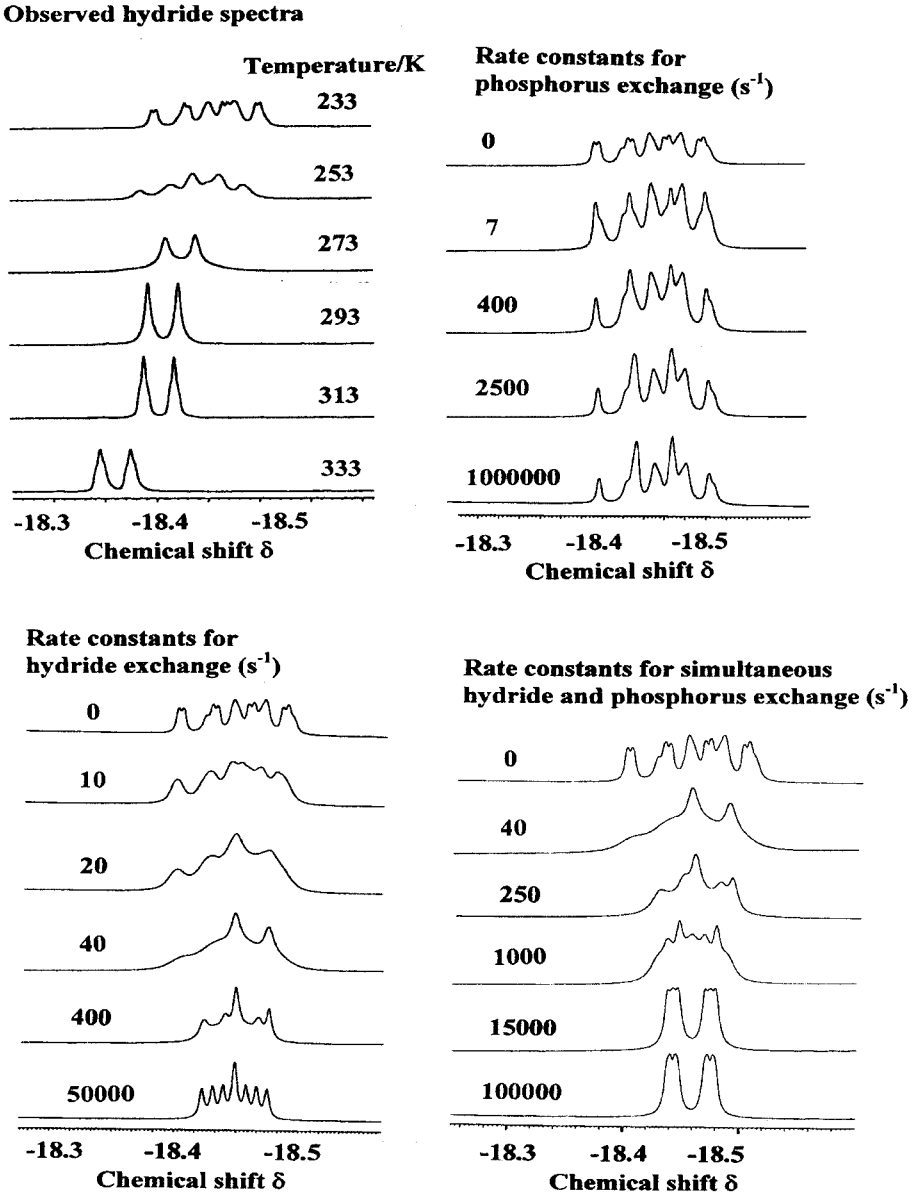

Figure 4. Top left: observed 500 MHz ^{1}H NMR spectra of $[Ru_3(\mu\text{-}H)_2(\mu_3\text{-}PPh)(CO)_7(\mu\text{-}dppm)]$ (**3**) in $CDCl_3$ in the hydride region recorded at various temperatures. Top right: Corresponding spectra of **3** simulated on the basis of exchange of the phosphorus nuclei of the dppm ligand without simultaneous exchange of the hydride ligands. Bottom left: corresponding spectra of **3** simulated on the basis of hydride exchange alone. Bottom right: corresponding spectra of **3** simulated on the basis of exchange of the hydride nuclei and exchange of the phosphorus nuclei both with the rate constants given.

Table 4. Chemical shifts (δ) and coupling constants (Hz) used for the 500-MHz NMR simulations for the compound $[Ru_3(\mu\text{-}H)_2(\mu\text{-}PPh)(CO)_7(\mu\text{-}dppm)]$ (**3**) at the lowest temperatures.

Nucleus		δ	Coupling constants with nucleus [Hz]			
			1	2	3	4
1	^{1}H	–18.450				
2	^{1}H	–18.466	1.00			
3	^{31}P	25.200	2.50	–13.00		
4	^{31}P	27.700	34.00	–13.50	59.7	
5	^{31}P	277.750	16.50	15.80	17.2	7.10

 © 2005 Wiley-VCH Verlag GmbH & Co. KGaA, Weinheim

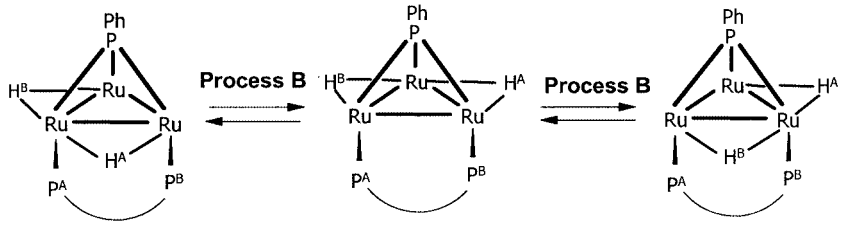

Scheme 3.

nous motion of both hydrides without the intermediate shown in Scheme 3. In this case there would be a transition state with a mirror plane.

In process B (or the modified single-step process described above) there is simultaneous exchange of H^A with H^B and of P^A with P^B, and Figure 4 shows the predicted outcome, again different to observed spectra. Process B does not lead to total exchange because, for example, H^A does not become equally correlated to P^A and to P^B. We have found that it is necessary to apply both processes A and B with different rates to obtain satisfactory correspondence of observed with calculated spectra. Figure 5 shows an excellent match, except that there is some observed drift of chemical shift with temperature which is not accounted for by exchange processes. It is surprising that there is such good correspondence, and we believe that this is because the H^A and H^B signals change chemical shifts in a similar way with changing temperature. A graphical presentation of these rate data is given in Figure 6. Note that the rates of process A obtained from a deconvolution of the two processes observed in the hydride spectra are closely similar to those obtained from the $^{31}P\{^1H\}$ spectra. Process B is about 5 times slower than process A and activation data for process **A** are $\Delta G^{\ddagger}$ = (52.2 ± 3.7) kJ·mol^{-1}, $\Delta H^{\ddagger}$ = (57.1 ± 3.7) kJ·mol^{-1}, $\Delta S^{\ddagger}$ = (16.7 ± 13.7) J·K^{-1}·mol^{-1} while those for process B are $\Delta G^{\ddagger}$ = (56.1 ± 3.0) kJ·mol^{-1}, $\Delta H^{\ddagger}$ = (60.0 ± 3.0) kJ·mol^{-1}, $\Delta S^{\ddagger}$ = (12.9 ± 9.6) J·K^{-1}·mol^{-1} The rate of migration of H^A from the most electron-rich site between the dppm-substituted Ru atoms is slower than migration of H^B which is in a less electron-rich site. However, the difference is very small, largely enthalpic and only represents a difference in $\Delta H^{\ddagger}$ of 2.9 kJ·mol^{-1}. A combination

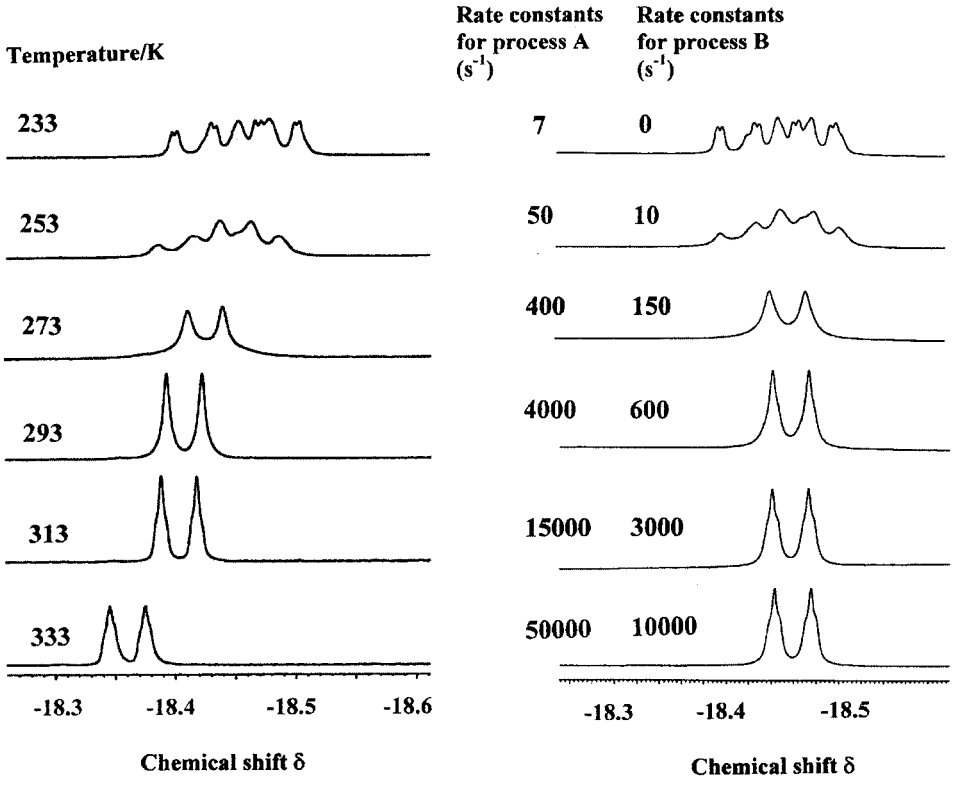

Figure 5. Left: observed 500 MHz ^1H NMR spectra of $[Ru_3(\mu\text{-}H)_2(\mu_3\text{-}PPh)(CO)_7(\mu\text{-}dppm)]$ (**3**) in $CDCl_3$ solution in the hydride region recorded at various temperatures. Right: corresponding spectra of **3** simulated on the basis of exchange by processes A and B with the rate constants given.

 © 2005 Wiley-VCH Verlag GmbH & Co. KGaA, Weinheim

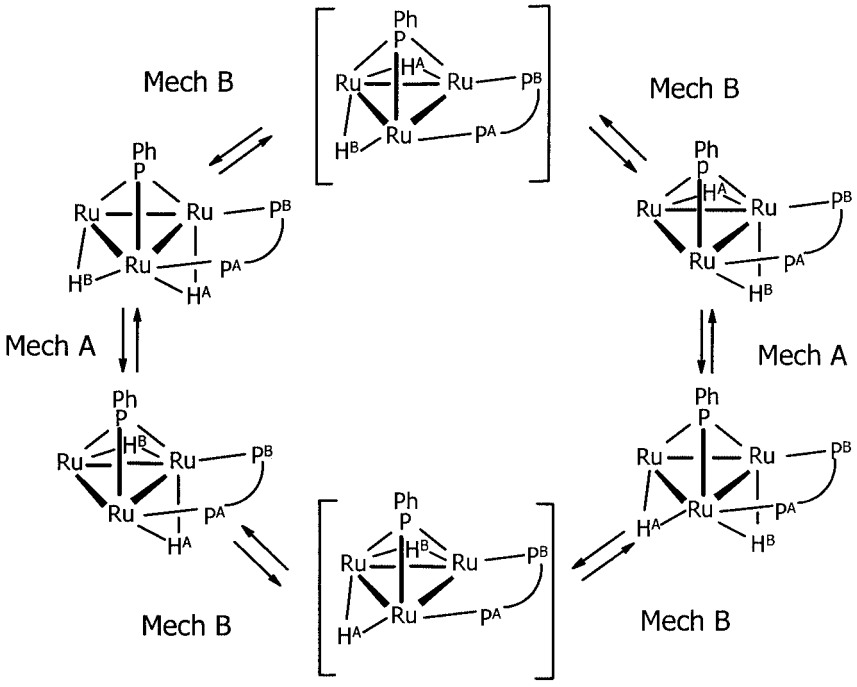

Scheme 4.

of processes A and B can be represented by Scheme 4. In the cycle each hydride jumps in turn and progresses through the three edges of the metal triangle.

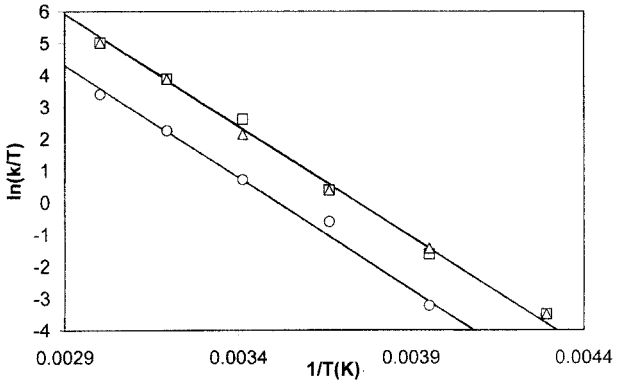

Figure 6. Graph of ln(k/T) for the processes **A** and **B** against (1/T)/K^{-1} for cluster [Ru_3(μ-H)$_2$(μ$_3$-PPh)(CO)$_7$(μ-dppm)] (**3**) in $CDCl_3$ solution. The rate of process **A** were obtained from the exchange of P nuclei observed in the $^{31}P\{^1H\}$ NMR spectrum (points Δ) and from ^1H NMR spectroscopic data (points □). Rates of process **B** were also obtained from ^1H NMR spectroscopic data (points ○).

Experimental Section

The compound [$Ru_3(CO)_{10}$(μ-dppm)] (**1**) was prepared according to the known method.[6] Infrared spectra were recorded with a Shimadzu FTIR 8101 spectrophotometer. ^1H and $^{31}P\{^1H\}$ NMR spectra were recorded with a Bruker DPX400 or DRX500 spectrometer.

Reaction of [$Ru_3(CO)_{10}$(μ-dppm)] (1) with $PPhH_2$: A 10% hexane solution of PH_2Ph (0.70 cm^3, 0.636 mmol) was added to a THF solution (35 cm^3) of **1** (0.205 g, 0.212 mmol) in a three-necked round-bottom flask. The reaction mixture was then refluxed for 6 h. The solvent was removed under reduced pressure and the residue was chromatographed by TLC on silica gel. Elution with cyclohexane/CH_2Cl_2 (7:3, v/v) developed two major and several very minor bands. The fastest moving band afforded unreacted **1** (0.005 g) and [Ru_3(μ-H)(μ-PHPh)(CO)$_8$(μ-dppm)] **2** (0.015 g, 7%) after fractional crystallization from hexane/CH_2Cl_2 at –15 °C.

Characterization of 2: $C_{39}H_{29}O_8P_3Ru_3$: calcd. C 45.84, H 2.87; found C 45.79, H 2.95. IR (νCO, CH_2Cl_2): $\tilde{\nu}$ = 2062 s, 2016 m, 1995 vs, 1950 m cm^{-1}. ^1H NMR ($CDCl_3$, 25 °C): δ = 4.26 (t, J = 10.8 Hz, 2 H), 7.35 (m, 26 H), –16.30 (t, J = 28.4 Hz, 1 H). FAB MS showed the parent molcular ion: m/z 1022. The second band yielded [Ru_3(μ-H)$_2$(μ$_3$-PPh)(CO)$_7$(μ-dppm)] (**3**) (0.042 g, 20%) as yellow crystals from hexane/CH_2Cl_2 at room temperature. $C_{38}H_{29}O_7P_3Ru_3$ calcd. C 45.92, H 2.95; found C 45.99, H 2.72. IR (νCO, CH_2Cl_2): $\tilde{\nu}$ = 2054 s, 2031 s, 1994 vs, 1985 sh, 1940 w cm^{-1}. FAB MS showed the parent molecular ion: m/z 994. The minor bands were too small for complete characterization.

Reaction of 1 with $PPhH_2$ in Presence of Me_3NO: To a dichloromethane solution (35 cm^3) of **1** (0.105 g, 0.109 mmol) was added a 10% hexane solution of $PPhH_2$ (0.24 cm^3, 0.218 mmol) followed by a dichloromethane solution (25 cm^3) of Me_3NO (0.017 g, 0.226 mmol). The reaction mixture was stirred at room temperature for 30 min. The solution was filtered through a short silica column, and the volatiles were removed under reduced pressure. Chromatographic separation as above developed one major and several minor bands. The major band gave unreacted **1** (0.010 g) and **2** (0.012 g, 11%) after fractional crystallization from hexane/CH_2Cl_2 at –4 °C. The minor bands were not completely characterized.

Conversion of 2 into 3: A THF solution of **2** (0.012 g, 0.012 mmol) was heated to reflux for 3 h. Removal of solvent under reduced pressure and chromatographic separation of the residue as above afforded **3** (0.007 g, 51%) as yellow crystals.

Synthesis of [Ru_3(μ-H)$_2$(μ$_3$-PPh)(CO)$_9$]: This cluster was prepared by a method modified from that in the literature. The cluster

 © 2005 Wiley-VCH Verlag GmbH & Co. KGaA, Weinheim

$[Ru_3(CO)_{12}]$ (0.252 g) was treated with equimolar PH_2Ph in cyclohexane at 60 °C for 45 min and then at 80 °C for 60 min. The product was separated by TLC on silica to give the product as yellow crystals (0.134 g, 51%) which were characterised by IR, MS, ^1H and ^{31}P NMR and by elemental analysis.

Synthesis of $[Ru_3(\mu\text{-}H)_2(\mu_3\text{-}PPh)(CO)_7(\mu\text{-}dppm)]$ from $[Ru_3(\mu\text{-}H)_2(\mu_3\text{-}PPh)(CO)_9]$: A standard procedure of preparing an acetonitrile derivative prior to substitution by phosphane was unsuccessful. Thus treatment of $[Ru_3(\mu\text{-}H)_2(\mu_3\text{-}PPh)(CO)_9]$ with $Me_3NO{\cdot}2H_2O$ in dichloromethane and acetonitrile did not form significant amounts of $[Ru_3(\mu\text{-}H)_2(\mu_3\text{-}PPh)(CO)_{9-x}(MeCN)_x]$, where $x = 1$ or 2. Treatment of the solution formed in this way with tertiary phosphanes did not give simple substitution products. Likewise visible photolysis of dichloromethane solutions of $[Ru_3(\mu\text{-}H)_2(\mu_3\text{-}PPh)(CO)_9]$ in the presence of dppm at room temperature did not lead to any significant reaction. However, direct thermal reaction of $[Ru_3(\mu\text{-}H)_2(\mu_3\text{-}PPh)(CO)_9]$ (0.0419 g) with dppm (0.0391 g) in refluxing cyclohexane (50 cm^3) under dinitrogen lead to the yellow solution becoming deep orange after 50 min. IR spectrsocopy indicated that most of the starting material had been consumed. Removal of the solvent under reduced pressure and separation of the residue by TLC [silica; eluent, petroleum ether (b. p. 40–60 °C)/dichloromethane, 3:1 by volume)] gave several bands. The major yellow band yielded $[Ru_3(\mu\text{-}H)_2(\mu_3\text{-}PPh)(CO)_7(\mu\text{-}dppm)]$ (**3**) as yellow crystals (0.020 g, 32%), whereas a minor yellow band gave $[Ru_3(\mu\text{-}H)_2(\mu_3\text{-}PPh)(CO)_8(\mu\text{-}dppm)]$ as a yellow solid (0.010 g, 16%). The latter compound has a similar IR spectrum [2072 w, 2047 m, 2038 vs, 2000 s, 1992 m cm^{-1} in cyclohexane] to monophosphane derivatives such as $[Ru_3(\mu\text{-}H)_2(\mu_3\text{-}PPh)(CO)_8(PMe_2Ph)]$[8] [2072 m, 2038 vs, 2003 m, 1989 m, 1973 cm^{-1} in cyclohexane], $[Ru_3(\mu\text{-}H)_2(\mu_3\text{-}PPh)(CO)_8(PH_2Ph)]$[2] [2077 m, 2048 s, 2041 s, 2009 s, 2001 m, 1993 m, 1978 w cm^{-1} in cyclohexane] and $[Ru_3(\mu\text{-}H)_2(\mu_3\text{-}PPh)(CO)_8(PMePh_2)]$.[9] Therefore, we believe the dppm is monodentate but we have not characterised the compound further.

X-Ray Crystal Structure Determinations for Compounds 2 and 3: Single crystals of compounds **2** and **3** were mounted on glass fibers and all geometric and intensity data were obtained with a Bruker SMART APEX CCD diffractometer using graphite-monochromated Mo-K_α radiation ($\lambda = 0.71073$ Å) at 150(2) K (compound **2**) and 293(2) K (compound **3**). Data reduction and integration was carried out with SAINT+ and absorption corrections were applied using the programme SADABS.[11,12] Structures were solved by Patterson synthesis for compound **2** or direct methods for compound **3** and developed using alternating cycles of least-squares refinement and difference-Fourier synthesis. All non-hydrogen atoms were refined anisotropically. Hydrogen atoms, except those bonded to ruthenium, were placed in calculated positions and their thermal parameters linked to those of the atoms to which they were attached (riding model). Hydrogen atoms bridging the ruthenium atoms were located and their positions refined using fixed isotropic thermal parameters. The SHELXTL PLUS V6.10 program package was used for structure solution and refinement.[13] General details: data collection method, ω rotation with narrow frames; absorption correction, semi-empirical from equivalents; refinement method, full-matrix least-squares on F^2.

CCDC-243253 (for **2**) and -243253 (for **3**) contain the supplementary crystallographic data for this paper. These data can be obtained free of charge from The Cambridge Crystallographic Data Centre via www.ccdc.cam.ac.uk/data_request/cif.

Acknowledgments

A. J. D. thanks the Wenner-Gren Foundation (Stockholm) for a fellowship to work with Dr. Nordlander at Lund University. Funds were also provided by the Royal Society (London) and the Swedish Academy of Sciences to support this collaboration. C. S. F. thanks the Chemistry Department, University College London for a teaching assistantship to carry out Ph. D. work. S. E. K. acknowledges the Royal Society for funds to work at UCL and the Swedish International Development Agency and the Swedish Science Research Council for support.

[1] a) Some recent examples: S. P. Tunik, T. S. Pilyugina, I. O. Koskevoy, S. I. Selivanov, M. Haukka, T. A. Pakkanen, *Organometallics* **2004**, *23*, 568; b) M. G. Ballinas-López, E. V. García-Báez, M. J. Rosales-Hoz, *Polyhedron* **2003**, *22*, 3403; c) T. Beringhelli, E. Cariati, C. Dragonetti, S. Galli, E. Lucenti, D. Roberto, A. Sironi, R. Ugo, *Inorg. Chim. Acta* **2003**, *354*, 79; d) G. Süss-Fink, L. Plasseraud, A. Maisse-François, H. Stoeckli-Evans, H. Berken, T. Fox, R. Gautier, J.-Y. Saillard, *J. Organomet. Chem.* **2000**, *609*, 196; e) M. P. Cifuentes, M. G. Humphrey, B. W. Skelton, A. H. White, *J. Organomet. Chem.* **1996**, *507*, 163; f) J. B. Keister, U. Frey, D. Zbinden, A. E. Merbach, *Organometallics* **1991**, *10*, 1497; g) L. R. Nevinger, J. B. Keister, *Organometallics* **1990**, *9*, 2313; h) P. Ewing, L. J. Farrugia, D. S. Rycroft, *Organometallics* **1988**, *7*, 859.

[2] F. Iwasaki, M. J. Mays, P. R. Raithby, P. L. Taylor, P. J. Wheatley, *J. Organomet. Chem.* **1981**, *213*, 185.

[3] S. P. Rowley, P. S. White, C. K. Schaver, *Inorg. Chem.* **1992**, *31*, 3158.

[4] E. Ngai-Man Ho, W.-T. Wong, *J. Chem. Soc., Dalton Trans.* **1998**, 51.

[5] a) A. Forster, B. F. G. Johnson, J. Lewis, T. W. Matheson, *J. Organomet. Chem.* **1976**, *104*, 225; b) J. Bracker-Novak, S. Hajela, M. Lord, M. Zhang, E. Rosenberg, R. Gobetto, L. Milone, D. Osella, *Organometallics* **1990**, *9*, 1379.

[6] M. I. Bruce, B. K. Nicholson, M. L. Williams, *Inorg. Synth.* **1989**, *26*, 276; M. I. Bruce, B. K. Nicholson, M. L. Williams, *Inorg. Synth.* **1990**, *28*, 225.

[7] A. J. Deeming, C. S. Forth, F. Rodgers, unpublished results.

[8] M. I. Bruce, O. Bin Shawkataly, M. L. Williams, *J. Organomet. Chem.* **1985**, *287*, 127.

[9] a) J. A. Clucas, M. M. Harding, A. K. Smith, *J. Chem. Soc., Chem. Commun.* **1985**, 1280; b) M. I. Bruce, E. Horn, O. Bin Shawkataly, M. R. Snow, E. Tiekink, M. L. Williams, *J. Organomet. Chem.* **1986**, *316*, 187; c) M. J. Stchedroff, S. Aime, R. Gobetto, L. Salassa, E. Nordlander, *Magnet. Reson. Chem.* **2002**, *40*, 107.

[10] gNMR, Ver. 4.1, Cherwell Scientific Ltd., Oxford, U. K., **1995**.

[11] SMART and SAINT software for CCD diffractometers, version 6.1, Bruker AXS, Madison, WI, **2000**.

[12] G. M. Sheldrick, SADABS software for empirical absorption correction, University of Göttingen, Germany, **2000**.

[13] G. M. Sheldrick, SHELXTL PLUS, version 6.1, Bruker AXS Inc., Madison, WI, **2000**.

Received: October 23, 2004
Published Online: September 13, 2005

 © 2005 Wiley-VCH Verlag GmbH & Co. KGaA, Weinheim